Soft Matter

PAPER

View Article Online
View Journal | View Issue

Cite this: *Soft Matter*, 2021, **17**, 5711

Elastic modulus distribution in poly(*N*-isopopylacrylamide) and oligo(ethylene glycol methacrylate)-based microgels studied by AFM†

Dimitri Wilms,* Yanik Adler, Fabian Schröer, Lennart Bunnemann and Stephan Schmidt

The spatial elastic modulus distribution of microgel networks in presence and absence of bifunctional crosslinkers is studied by AFM. Thermoresponsive poly(*N*-isopopylacrylamide) (PNIPAM) and poly(2-(2-methoxyethoxy)ethyl methacrylate-*co*-oligo(ethylene glycol)methacrylate) (P(MEO_2MA-*co*-OEGMA)) microgels are synthesized *via* precipitation polymerization above their lower critical solution temperature (LCST). High-resolution elastic modulus profiles are acquired using AFM force-indentation mapping of surface-deposited microgels at 25 °C. For both microgel systems, the use of a bifunctional crosslinker leads to a strong elastic modulus gradient with stiff microgel cores and soft networks toward the edge. In absence of a dedicated crosslinker (self-crosslinking), PNIPAM microgels show a homogeneous elastic modulus distribution, whereas self-crosslinked P(MEO_2MA-*co*-OEGMA) microgels still show decreasing elastic moduli from the centre to the edge of the microgels. However, POEGMA microgels without comonomer showed no elastic modulus gradient suggesting that different incorporation rates of MEO_2MA and OEGMA result in a radial variation of the polymer segment density. In addition, when varying the molecular weight of OEGMA the overall elastic modulus was affected, possibly due to molecular weight-dependent phase behavior and different reactivity. This shows that quite different microgel architectures can be obtained by the simple "one-pot" precipitation reaction of microgels which may open to new avenues toward advanced applications.

Received 25th February 2021,
Accepted 13th May 2021

DOI: 10.1039/d1sm00291k

rsc.li/soft-matter-journal

Introduction

Micro and nanoparticles composed of stimuli responsive polymers paved the way toward several promising applications, such as triggered drug delivery systems,[1–5] materials with advanced optical properties,[6,7] or bioactive coatings that are capable of responding to environmental parameters.[8–13] A very prominent type of responsive microparticles are thermosensitive microgels composed of polymers with a lower critical solution temperature (LCST).[14] When increasing the temperature above the LCST, the swollen microgels collapse due to the formation of polymer–polymer contacts and the partial removal of the hydration layer surrounding the polymer chains. In comparison to macroscopic polymer gels, microgels show a range of interesting properties, such as rapid and strong volume changes upon temperature variation, narrow size distribution, and straightforward processing toward coatings.[15–18] In addition, their synthesis *via* free radical polymerization is comparatively simple. Such microgels are often composed of polymers with an LCST in the physiological temperature range, *e.g.* poly(*N*-isopropylacrylamide) (PNIPAM) or 2-(2-methoxyethoxy) ethyl methacrylate and oligo(ethylene glycol) methacrylate (P(MEO_2MA-*co*-OEGMA)).[14,19] In a single precipitation polymerization step in water above the polymer's LCST, the monomers are reacted in presence of a crosslinker to form monodisperse microgels with diameters of a few hundred nanometers. For crosslinking, bifunctional acrylamides or acrylates are typically used. Since the crosslinkers are bivalent they tend to be incorporated at higher rates into the growing microgels during precipitation polymerization, leading to higher crosslinking in the microgel centre.[20,21] The resulting microgels show a crosslinking density gradient, *i.e.* a stiff, highly crosslinked core with a soft and very fuzzy outer perimeter due to low crosslinking.[22–24] For some applications, *e.g.* in drug release or tissue engineering, different network structures and higher overall deformability are required. To address these needs, hollow microgels and ultra-soft microgels have been developed.[25,26] It has been shown that such microgel structures can be obtained by omitting bifunctional crosslinkers but instead using chain transfer

Institute for Organic Chemistry and Macromolecular Chemistry, Heinrich-Heine-University, Universitätsstr. 1, 40225 Düsseldorf, Germany. E-mail: dimitri.wilms@hhu.de

† Electronic supplementary information (ESI) available. See DOI: 10.1039/d1sm00291k

reactions to introduce crosslinks in the microgel network during the precipitation reaction procedure.[27] Such microgels can be considered "self-crosslinked" due to the absence of dedicated crosslinker molecules.

As of yet, such self-crosslinked, ultra-soft microgels were largely based on PNIPAM.[26–30] For biomedical applications where the toxicity of the microgels' degradation products is a concern,[31] microgels with a polyethylene glycol (PEG)-based backbone are favoured instead.[32,33] A pioneering study has confirmed the feasibility of self-crosslinked OEGMA-based microgels.[24] Therefore, in this study the network structure of self-crosslinked P(MEO_2MA-*co*-OEGMA) microgels of varying composition is investigated and compared to self-crosslinked PNIPAM microgels. In addition, a systematic comparison between self-crosslinked microgels and microgels crosslinked by bivalent crosslinkers is presented. As a tool to determine the network structure we use AFM force-indentation measurements, which give the elastic modulus of the microgel network and the crosslinking density at a resolution in the nanometer range.

Experimental section

Microgel synthesis

PNIPAM microgels with crosslinker were synthesized *via* surfactant-free non-stirred precipitation polymerization as described by Richtering and coworkers[34] (Table 1). *N*-Isopropylacrylamide (Sigma-Aldrich, >95%), *N*,*N*′-methylenebisacrylamide (Sigma-Aldrich, 99.5%) and ammonium peroxodisulfate (APS, Sigma-Aldrich, >99%) were used without further purification. For self-crosslinked PNIPAM microgels, NIPAM was dissolved in 20 mL ultra-pure water (1.4 mmol, 0.07 mol L^{-1}) and heated to 70 °C while purging with N_2 followed by adding APS dissolved in 1 mL ultra-pure water (0.06 mmol, 0.003 mol L^{-1}) after 30 min. The reaction was terminated by cooling in an ice bath after reacting at 70 °C under N_2 atmosphere for 16 h. To remove any unreacted or loose polymer the particles were washed by repeated centrifugation at 10 000*g* for 1 hour. In a final step the particles were freeze dried. Four different P(MEO_2MA-*co*-OEGMA) microgel samples were prepared by surfactant free emulsion polymerization. The presence of crosslinker (ethylene glycol dimethacrylate, EGDMA), comonomer (MEO_2MA), and the molecular weight of OEGMA (300 g mol^{-1}, $OEGMA_{300}$ and 500 g mol^{-1}, $OEGMA_{500}$) was varied. OEGMA and EGMA (TCI Germany GmbH) the initiator potassium peroxodisulfate (KPS) and EGDMA (>95%, Sigma-Aldrich, Germany) were used without further purification. The monomers were dissolved in 84 mL of ultra-pure water and purged with N_2 for 30 min while stirring and heating to 80 °C followed by adding KPS dissolved in 1 mL ultra-pure water (0.255 mmol, 0.003 mol L^{-1}). The reaction was stopped after 6 hours by cooling down in an ice bath. The microgels were purified by repeated centrifugation at 10 000*g* for 2–3 hours.

Table 1 Composition of the microgel reaction mixture, the hydrodynamic radius (R_h) and the ratio of R_h above and below the LCST (swelling ratio) as measured by dynamic light scattering (DLS) (see ESI, S1). Microgels prepared without crosslinker (self-crosslinked) are termed "SCL". Microgels prepared with crosslinker are termed according to the crosslinker ("BIS" or "EGDMA")

Microgel sample	Monomer [mmol]	Crosslinker [mmol]	R_h [nm]	Swelling ratio
$PNIPAM_{BIS}$	6.19	0.32 (5 mol%)	350	2.5
$PNIPAM_{SCL}$	70	—	429	3.7
P(MEO_2MA-*co*-$OEGMA_{300}$)$_{SCL}$	8.13/0.9[a]	—	197	2.3
P($OEGMA_{300}$)$_{SCL}$	80.7	—	575	2.1
P(MEO_2MA-*co*-$OEGMA_{500}$)$_{EGDMA}$	8.13/0.9[a]	0.09 (1 mol%)	125	1.5
P(MEO_2MA-*co*-$OEGMA_{500}$)$_{SCL}$	8.13/0.9[a]	—	195	2.1

[a] Ratio of OEGMA/MEO_2MA.

Microgel surface deposition

Glass slides were cleaned by Hellmanex III solution and subsequently treated in a solution of water, hydrogen peroxide (30%) and ammonia (25%) at a 5 : 1 : 1 ratio at 70 °C for 30 min. After rinsing, the surfaces were used immediately for microgel deposition (0.1 wt%) *via* spin coating at 2000 rpm for 60 s.

Atomic force microscopy (AFM)

AFM measurements were performed on a JPK NanoWizard IV in quantitative imaging (QI™) mode with a setpoint force of 5 nN, a loading rate of about 175 μN s^{-1} curve, and a sampling rate of 40 kHz. Cantilevers (HQ:XSC11/No Al, μMasch, Bulgaria) with a nominal spring constant of 7 N m^{-1} were used. The AFM tip radius was obtained by imaging a porous alumina surface (PA01, μMasch, Bulgaria) and evaluation with Gwyddion.[35] Measurements were conducted in ultra-pure water at 20 °C. The obtained force–deformation maps were processed with the software provided by the AFM manufacturer to calculate the elastic modulus by fitting the approach cycle with the Hertzian model. To account for the limited thickness of the microgel layer selected force curves were fitted with the Dimitriadis model using the microgel thickness at the respective radial position to calculate corrected elastic moduli.[36] The fit range was limited by choosing a maximum indentation depth, which was up to 10–50% of the microgel thickness depending on how well the fits represented the data. Radial profiles of the elastic moduli maps from at least six similar-sized microgels were using the radial profile plugin for ImageJ.[37] Single pixels with elastic moduli greater than 100 MPa (outliers) were excluded from the analysis.

Results and discussion

High-resolution elastic modulus mapping

To determine the crosslinking gradient and the overall network structure we perform AFM nanoindentation measurements, which allow to map the elastic modulus on a nanometer scale. The elastic modulus can be directly related to the density of polymer crosslinks in a gel: The density of crosslinks in a polymer network with an average mesh width ξ is proportional to ξ^{-3}. According to de Gennes,[38,39] for polymer networks in

good solvents the concentration of polymer segments between crosslinks C scales with ξ as

$$\xi \sim C^{-3/4} \quad (1)$$

and the elastic modulus E is proportional to the density of crosslinks

$$E \sim \xi^{-3} \sim C^{9/4}. \quad (2)$$

Therefore, the polymer gel's elastic modulus as determined by AFM is a measure of the polymer segment concentration and crosslinking density of the gel. Previous work showed that AFM nanoindentation measurements on adsorbed BIS-crosslinked PNIPAM microgels reveal radial elastic modulus gradients, where higher elastic moduli were found in the centre of the microgels.[9,22,40] Following these studies, the AFM investigations were also conducted with adsorbed microgels on glass slides in water. High-resolution AFM force–deformation mapping was performed followed by fitting the force-indentation traces with the Hertzian model of elastic contacts to obtain the elastic modulus E:

$$F = \frac{4{r_{\mathrm{tip}}}^{1/2} d^{3/2}}{3(1-\nu^2)}, \quad (3)$$

where r_{tip} is the radius of the cantilever tip, ν the Poisson ratio, d the sample deformation, and F the applied force. This analysis yields high-resolution maps of the elastic modulus, *e.g.* for a $P(MEO_2MA\text{-}co\text{-}OEGMA_{500})_{SCL}$ microgel as shown in Fig. 1a. For further analysis, radial averages of the elastic moduli were calculated and plotted against the radial position where the origin is the centre of the microgels (Fig. 1b). To account for the finite thickness h of the microgel on the solid support, the force curves were additionally fitted using Dimitriadis' model (with ν set to 0.5) to obtain the corrected elastic modulus $E_{\mathrm{corrected}}$:

$$F = f_{\mathrm{correction}} \cdot \frac{16{r_{\mathrm{tip}}}^{1/2} d^{3/2}}{9} E_{\mathrm{corrected}}, \quad (4)$$

where $f_{\mathrm{correction}}$ is defined as

$$f_{\mathrm{correction}} = 1 + 0.884\chi + 0.781\chi^2 + 0.386\chi^3 + 0.0048\chi^4, \quad (5)$$

with χ defined as

$$\chi = \frac{\sqrt{r_{\mathrm{tip}} d}}{h}. \quad (6)$$

Selected force curves taken at certain radial positions giving similar (uncorrected) elastic moduli as compared to the radial averages were fitted again with the Dimitriadis model to obtain the corrected elastic modulus profiles (Fig. 1b).

Elastic modulus gradients of PNIPAM microgels

The well-studied BIS-crosslinked $PNIPAM_{BIS}$ microgels were compared against self-crosslinked $PNIPAM_{SCL}$ microgels prepared in absence of BIS where crosslinking takes place by chain transfer reactions. For an initial overview, three force-deformation curves taken at the centre, the very edge, and between the edge and centre are shown (Fig. 2a). The elastic moduli obtained at the centre of $PNIPAM_{SCL}$ microgels were an order of magnitude smaller compared to $PNIMAP_{BIS}$, suggesting a reduced network density for $PNIPAM_{SCL}$ due to the absence of a dedicated crosslinker (Table 2). An additional indication of the strongly reduced network density of $PNIPAM_{SCL}$ is very their flat, pancake-like shape in the adhered state on the glass slide. Due to their higher crosslinking density adhered $PNIPAM_{BIS}$ microgels attain truncated sphere shapes, with a peak height of 120 nm. As expected, the swelling behaviour of the microgels is affected by the overall

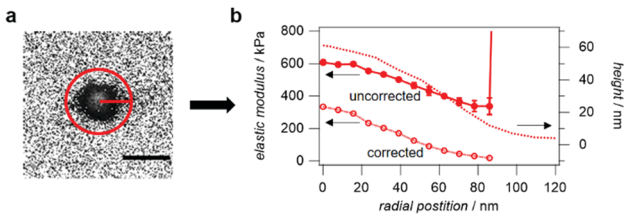

Fig. 1 High resolution elastic modulus maps and calculation of radial profiles. (a) An elastic modulus map of a single $P(MEO_2MA\text{-}co\text{-}OEGMA_{500})_{SCL}$ microgel particle (scale bar is 200 nm). The red circle indicates the range over which the elastic modulus distribution is averaged at certain radial positions to create a radial profile. (b) The resulting elastic modulus profile, ranging from the centre to the edge of the microgels (full circles, left axis). Additionally, the elastic modulus values were corrected according to the Dimitriadis model (hollow circles, left axis). The height profile was reconstructed from the high-resolution force maps (dashed line, right axis).

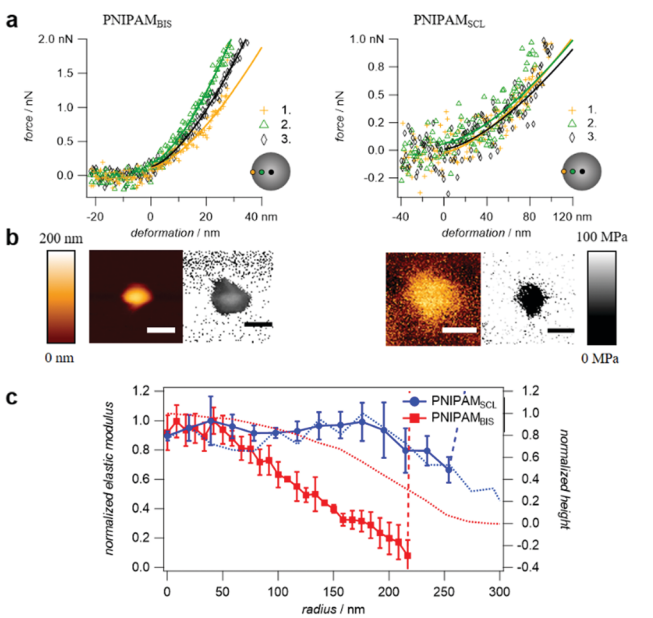

Fig. 2 The elastic moduli of deposited PNIPAM microgels as a function of the radial position. (a) Typical AFM force–distance measurements at the microgel centre (black), between centre and edge (blue) and the edge (red) for $PNIPAM_{BIS}$ (left) and $PNIPAM_{SCL}$ (right). (b) Typical topography and elastic modulus images of a single PNIPAM microgel. Scale bars: 200 nm. (c) Plot of the elastic modulus *vs.* the radial position calculated from at least five microgels using high-resolution elastic modulus mapping and height trace (dashed lines) reconstructed from vertical tip position during force map acquisition.

Table 2 Elastic moduli comparison from AFM indentation measurements taken at the microgels' apex

Microgel sample	Elastic modulus at centre [kPa]
$PNIPAM_{BIS}$	340 ± 10
$PNIPAM_{SCL}$	13 ± 3
$P(MEO_2MA\text{-}co\text{-}OEGMA_{500})_{EGDMA}$	63000 ± 500
$P(MEO_2MA\text{-}co\text{-}OEGMA_{500})_{SCL}$	850 ± 6
$P(MEO_2MA\text{-}co\text{-}OEGMA_{300})_{SCL}$	292 ± 2
$P(OEGMA_{300})_{SCL}$	123 ± 6

crosslinking density, where $PNIPAM_{SCL}$ showed a significantly stronger collapse when increasing the temperature above the LCST (ESI,† S1). The detailed distribution of the elastic moduli and particle height on the solid surface was read from high-resolution AFM force maps. In agreement with recent work by Richtering and coworkers,[28] the $PNIPAM_{SCL}$ microgels showed only small changes of the elastic modulus across the microgel, whereas the elastic modulus decreased toward the edge of $PNIPAM_{BIS}$ microgels as found in earlier studies.[9,22] From the apex to radii of about 50 nm, the elastic modulus of $PNIPAM_{BIS}$ was constant indicating a homogeneous crosslinking density in the core region, which was also observed in scattering experiments and in super-resolution microscopy.[41,42] However, here the core region appeared smaller owing to scanning only the microgel surface by AFM indentation. In absolute numbers, the elastic moduli of $PNIPAM_{BIS}$ of 350 kPa in the microgel centre were a factor of 3 larger compared to previous work.[9,28] The higher values could be attributed to several factors. For example, to achieve reasonable acquisition times of the high-resolution force maps, the force curves were recorded at high speed using loading rates on the order of 500 μN s^{-1}. Due to viscoelastic and hydrodynamic effects, the stiffness of hydrogels increases at high loading rates.[43,44] In addition, the microgels were dried to immobilize them on the solid support. This may lead to an increase in network density even after rehydration since the network could stay partially adhered to the support. This results in overall increased elastic moduli compared to immobilization techniques that work without drying. Compared to previous work on self-crosslinked microgels,[45] here the molar ratio of NIPAM and peroxydisulfate initiator was 3-times larger leading to increased crosslinking and to a stiffness of the $PNIPAM_{SCL}$ microgels. Overall, the results confirmed that $PNIPAM_{BIS}$ radial density gradients owing to the increased incorporation rate of BIS compared to NIPAM. Microgels synthesized under self-crosslinking show a homogeneous segment concentration across the microgel.

Elastic modulus gradients of oligo(ethylene glycol)-based microgels

Different classes of oligo(ethylene glycol)-based microgels were prepared: (1) with comonomer and crosslinker ($P(MEO_2MA\text{-}co\text{-}OEGMA)EGDMA$), (2) with comonomer and without crosslinker ($P(MEO_2MA\text{-}co\text{-}OEGMA)_{SCL}$), (3) without comonomer or crosslinker ($POEGMA_{SCL}$). In addition, the OEGMA molecular weight was varied ($OEGMA_{300}$, $OEGMA_{500}$). First the microgels synthesized with crosslinker and comonomer are discussed. Most frequently studied are $P(MEO_2MA\text{-}co\text{-}OEGMA)EGDMA$ microgels with 1–5 mol% EGDMA crosslinker and a MEO_2MA/OEGMA ratio of about 9 : 1 because these microgels show an LCST in the physiological range and swelling properties that are comparable to $PNIPAM_{BIS}$ microgels.[19] Under the drying deposition method used here, the $P(MEO_2MA\text{-}co\text{-}OEGMA_{500})EGDMA$ microgels showed large elastic moduli in the centre, on the order of 60 MPa, that were strongly decreasing toward the edge of the microgel (Fig. 3, left). Starting at a radial position of 50 nm, the elastic modulus trace showed an extended plateau where the elastic modulus was constant, about 20% compared to the maximum in the centre. This plateau coincides with a flat hairy-like structure seen in AFM images (ESI,† S4). The very high elastic modulus in the centre as well as the radial gradient in elastic modulus could be explained with the different reactivity of the three methacrylate reactants MEO_2MA, $OEGMA_{500}$ and EGDMA. MEO_2MA-rich domains with increased crosslinking density and stiffness are expected to form in the centre of the microgels owing to the increased reactivity of the crosslinker EGDMA, the fast diffusion rate and increased reactivity of the short monomer MEO_2MA, as well as the phase behaviour of MEO_2MA oligomers. EGDMA is known to exhibit an increased reactivity compared to BIS,[46] leading to small high-density cores and absence of an extended constant crosslinking region in the microgels centre. Regarding the phase behaviour, MEO_2MA oligomers have a lower LCST compared to OEGMA oligomers.[47] Therefore it is likely that stiff MEO_2MA-rich domains form in the beginning of the reaction that constitute the centre of the

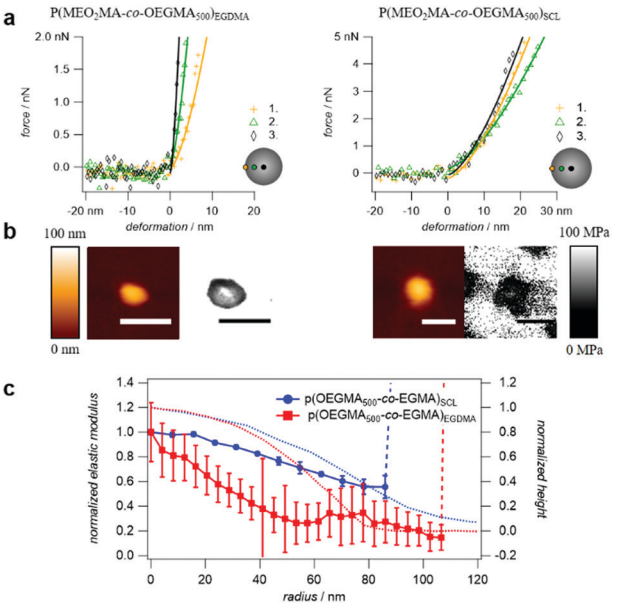

Fig. 3 The elastic moduli of $P(MEO_2MA\text{-}co\text{-}OEGMA_{500})_{EGDMA}$ and $P(MEO_2MA\text{-}co\text{-}OEGMA_{500})_{SCL}$ microgels as a function of the radial position. (a) Typical AFM force–distance measurements at the microgel centre (black), between centre and edge (blue) and the edge (red) for $P(MEO_2MA\text{-}co\text{-}OEGMA)_{EGDMA}$ (right) and $P(MEO_2MA\text{-}co\text{-}OEGMA_{500})_{SCL}$ (left). (b) Typical topography and elastic modulus images of a single microgel. Scale bars: 200 nm. (c) Plot of the elastic modulus *vs.* the radial position calculated from at least six microgels using high-resolution elastic modulus mapping and height traces (dashed lines) reconstructed from vertical tip position during force map acquisition.

microgels. Indeed, using neutron scattering, Wellert and co-workers found high density inhomogeneities in EGDMA-crosslinked P(MEO_2MA-*co*-OEGMA) microgels which they interpreted as MEO_2MA rich-domains forming during the reaction.[21] Overall, these results suggest that the observed radial elastic modulus gradients for P(MEO_2MA-*co*-$OEGMA_{500}$)$_{EGDMA}$ microgels are not only due to the increased reactivity of the bivalent crosslinker but also due to different monomer diffusion rates and phase behaviour of the oligomeric methacrylates forming during the reaction.

To confirm this observation, we analysed the P(MEO_2MA-*co*-$OEGMA_{500}$)$_{SCL}$ microgels prepared in absence of crosslinker while maintaining the 9 : 1 ratio between MEO_2MA and OEGMA monomers (Fig. 3, right). The absence of a bifunctional crosslinker resulted in overall softer microgels and also the very stiff core regions found in P(MEO_2MA-*co*-$OEGMA_{500}$)$_{EGDMA}$ microgels were not present. Interestingly, the force curves and high-resolution maps showed a radial elastic modulus gradient although a crosslinker was absent (Fig. 3, right). The elastic modulus decreased to 60% from centre to edge, a lower gradient compared to microgels prepared with crosslinker. Both MEO_2MA and $OEGMA_{500}$ are monofunctional and have the same reactive groups. Therefore, the elastic modulus gradient is perhaps due to an increased diffusion rate of MEO_2MA compared to $OEGMA_{500}$ in addition to differences in phase behaviour of the various oligomers formed during the reaction (Fig. 5). Owing to the smaller LCST of MEO_2MA-rich oligomers compared to OEGMA-rich oligomers, MEO_2MA is incorporated faster in the seed particles formed at the early stages of the reaction. On the other hand, since OEGMA is incorporated at slower rates OEGMA-rich domains are formed at the outer radii of the microgels. Given the longer side chain and the increased sterical repulsion of OEGMA compared MEO_2MA a decreasing density of polymer segments and a lower elastic modulus toward the edge of the microgels is observed.

From the analysis of the self-crosslinked samples P(MEO_2MA-*co*-$OEGMA_{500}$)$_{SCL}$ and $PNIPAM_{SCL}$ one could expect that a homogeneous elastic modulus distribution can only be achieved by using a single type of monomer for microgel synthesis. To test this, we compared microgels prepared by homopolymerization, P($OEGMA_{300}$)$_{SCL}$, with microgels prepared by copolymerization, P(MEO_2MA-*co*-$OEGMA_{300}$)$_{SCL}$ (Fig. 4). $OEGMA_{300}$ readily forms monodisperse microgels by homopolymerization using the standard precipitation polymerization method.[24] This allows for the synthesis of poly(oligo ethylene) microgels consisting of only one, self-crosslinked monomer, which could not be achieved with $OEGMA_{500}$. Typical force curves at different positions on individual particles and high resolution force maps showed that P($OEGMA_{300}$)$_{SCL}$ had no elastic modulus gradient while the copolymerized microgel P(MEO_2MA-*co*-$OEGMA_{300}$)$_{SCL}$ showed decreasing elastic moduli toward the edge of the microgels, quite similar to the P(MEO_2MA-*co*-$OEGMA_{500}$)$_{SCL}$ microgels. The elastic modulus at the microgels' apex was larger for P(MEO_2MA-*co*-$OEGMA_{500}$)$_{SCL}$ compared to P(MEO_2MA-*co*-$OEGMA_{300}$)$_{SCL}$ (Table 2).

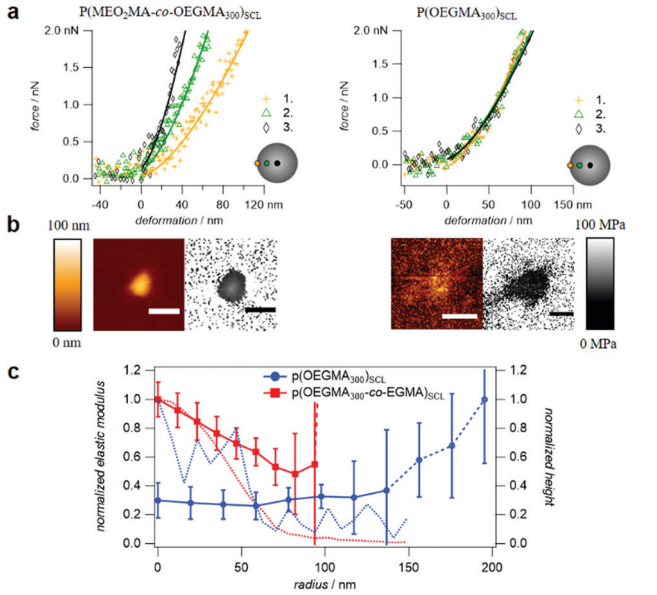

Fig. 4 The elastic moduli of P(MEO_2MA-*co*-$OEGMA_{500}$)$_{SCL}$ and P($OEGMA_{500}$)$_{SCL}$ microgels as a function of the radial position. (a) AFM force–indentation measurements at the microgel centre (black), between centre and edge (blue) and the edge (red) for P(MEO_2MA-*co*-$OEGMA_{300}$)$_{SCL}$ (right) and P($OEGMA_{300}$)$_{SCL}$ (left). (b) Typical topography and elastic modulus images of a single microgel. Scalebars: 200 nm. (c) Plot of the elastic modulus *vs.* the radial position (left) calculated from at least five microgels using high-resolution elastic modulus mapping (right).

The increased elastic modulus of P(MEO_2MA-*co*-$OEGMA_{500}$)$_{SCL}$ compared to P(MEO_2MA-*co*-$OEGMA_{300}$)$_{SCL}$ could be explained by a reduced incorporation of $OEGMA_{500}$ in relation to $OEGMA_{300}$ since larger contents of OEGMA should lead to increased excluded volume and softer networks. A less effective incorporation of the larger $OEGMA_{500}$ monomer could be caused by a lower diffusion rate and lower reactivity owing to the increased molecular weight and sterical shielding. In addition, the different LCSTs of $OEGMA_{500}$-rich and $OEGMA_{300}$-rich oligomers[47] that may form to a certain extent at the beginning of the reaction may affect the overall incorporation of OEGMA. While $OEGMA_{500}$-rich oligomers have an LCST above the reaction temperature (80 °C) reducing their incorporation in the growing microgel networks, the $OEGMA_{300}$-rich oligomers have an LCST below the reaction temperature and undergo a phase transition enabling increased incorporation in the microgel network (Fig. 5). This leads to a higher OEGMA content and lower elastic moduli for P(MEO_2MA-*co*-$OEGMA_{300}$)$_{SCL}$ microgels compared to P(MEO_2MA-*co*-$OEGMA_{500}$)$_{SCL}$.

Overall, quite different elastic moduli distributions prepared by radical precipitation polymerization of microgels can be achieved by varying the type and composition of monomers. Homogeneous crosslinking could only be achieved *via* self-crosslinking and homopolymerization. It was also notable that the elastic modulus of P($OEGMA_{300}$)$_{SCL}$ was lower compared to $PNIPAM_{SCL}$ (Table 2). This is likely due to an increased amount of persulfate initiator for the synthesis of $PNIPAM_{SCL}$ (1 mol%) compared to P($OEGMA_{300}$)$_{SCL}$ (0.5 mol%). The amount of initiator was chosen to obtain microgels of similar size, where

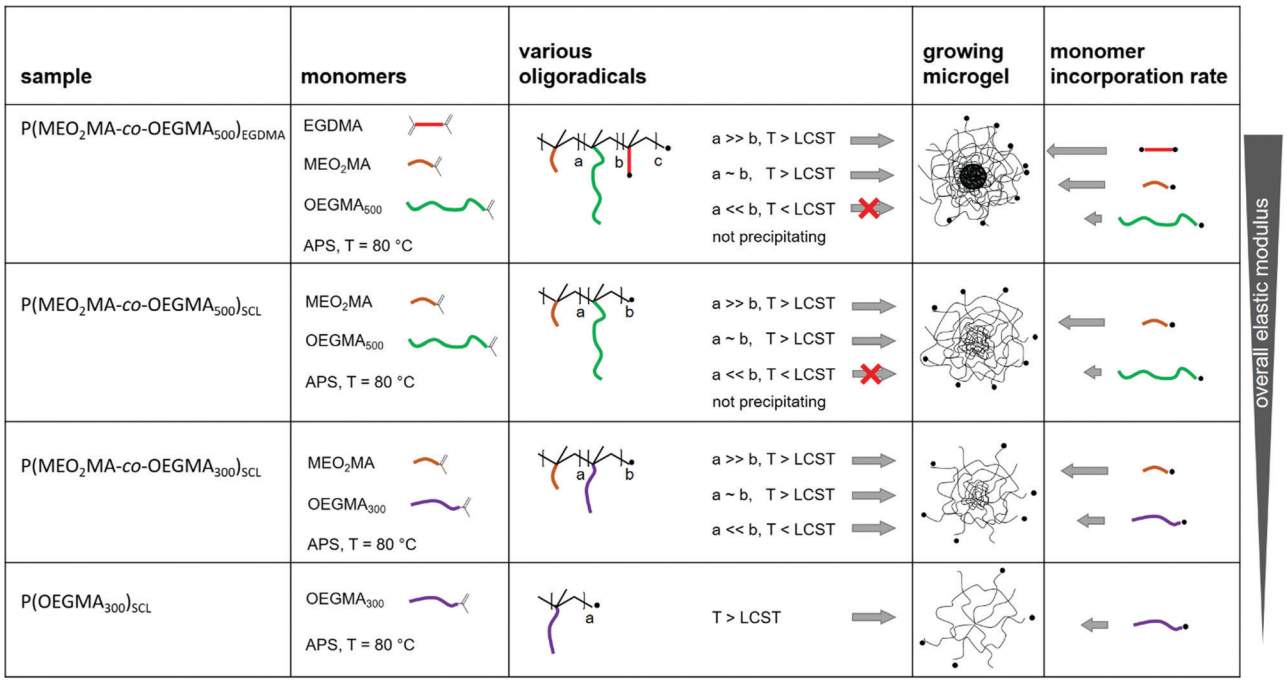

Fig. 5 Overview of the proposed mechanisms for the elastic modulus gradient and the different overall elastic moduli of oligo(ethylene glycol)-based microgels. The reactivity and diffusion rate of MEO_2MA is larger when compared to OEGMA. In addition, MEO_2MA-rich oligomers have a low LCST, which leads to dense domains in presence of a bifunctional crosslinker and elastic modulus gradients when copolymerized with OEGMA even in absence of a crosslinker. Consequently, the homopolymerization of $OEGMA_{300}$ results in microgels without elastic modulus gradient. For $P(MEO_2MA\text{-}co\text{-}OEGMA_{300})_{SCL}$ all possible oligomers that can form have an LCST below 80 °C whereas $OEGMA_{500}$-rich oligomers have an LCST above 80 °C and do not precipitate during the reaction. Considering the larger reactivity of $OEGMA_{300}$ when compared to $OEGMA_{500}$ this leads to an increased $OEGMA_{300}$ incorporation and lower overall elastic moduli for $P(MEO_2MA\text{-}co\text{-}OEGMA_{300})_{SCL}$ when compared to $P(MEO_2MA\text{-}co\text{-}OEGMA_{500})_{SCL}$.

adding more initiator typically leads to a size increase.[34] Nevertheless the increased elastic modulus for $PNIPAM_{SCL}$ may be due to intrinsic effects, *e.g.* the large side chains of the $OEGMA_{300}$ may add to free volume and an overall lower density of polymer segments compared to NIPAM. In addition, the amide groups in PNIPAM are likely to interact due to hydrogen bonding, whereas $OEGMA_{300}$ lacks hydrogen bond donating groups thus showing a lower network density and a lower elastic modulus.

Conclusions

We aimed to investigate the spatial elastic modulus distribution of soft colloidal thermoresponsive microgels adsorbed at a solid surface as a function of the monomer composition. For this purpose, two classes of microgels composed of PNIPAM or $P(MEO_2MA\text{-}co\text{-}OEGMA)$ were prepared in absence or presence of a bifunctional crosslinker. Elastic modulus maps were collected by high-resolution AFM force–indentation measurements. The studied PNIPAM microgel systems confirmed previous results, *i.e.* the presence of a crosslinker results in a strong radial elastic modulus gradient with decreasing elastic modulus from centre to edge,[23] whereas self-crosslinked PNIPAM microgels showed no elastic modulus gradient.[28] The elastic modulus gradients obtained for the crosslinker are likely due to the increased reactivity compared to NIPAM owing to the bivalent structure of the crosslinker. On the other hand, self-crosslinked $P(MEO_2MA\text{-}co\text{-}OEGMA)$ showed a clear elastic modulus gradient, suggesting that MEO_2MA is incorporated at higher rates compared to OEGMA. This leads to enrichment of OEGMA at the outer perimeter of the microgels and lower elastic moduli from centre to edge due to the increased excluded volume of OEGMA compared to MEO_2MA. Consequently, in absence of MEO_2MA, the homopolymerization of OEGMA leads to microgels without elastic modulus gradient and very soft networks compared to self-crosslinked PNIPAM microgels due to the absence of hydrogen bonding between the polymer segments. Upon varying the molecular weight of OEGMA the elastic modulus of $P(MEO_2MA\text{-}co\text{-}OEGMA)$ can be tuned further, where increased chain lengths lead to a decreased incorporation of OEGMA and increased stiffness. This might be due to a combination of effects, such as differences in reactivity and phase behaviour upon varying the OEGMA molecular weight. Importantly, $P(MEO_2MA\text{-}co\text{-}OEGMA)$ microgels synthesized with bifunctional crosslinkers showed very stiff cores, which are likely due to phase separation of MEO_2MA during the reaction as observed earlier.[21] This overall shows that quite different network architectures can be established by mere variation of the monomer composition *via* a simple one-step precipitation reaction procedure. This may offer new prospects toward microgels and coatings with well-defined nanometer-scale material properties for advanced applications.

Conflicts of interest

There are no conflicts to declare.

Acknowledgements

The authors acknowledge funding by the German Research foundation (DFG) in the project SCHM 2748/5-1. We thank Prof. Dr. Matthias Karg (Institute of Physical Chemistry I, Heinrich-Heine-University Duesseldorf) for providing the instrumetation for the high-resolution elastic modulus mapping.

References

1 B. Sung, M. H. Kim and L. Abelmann, *Bioeng. Transl. Med.*, 2021, **6**, e10190, DOI: 10.1002/btm2.10190.
2 A. S. Caldwell, B. A. Aguado and K. S. Anseth, *Adv. Funct. Mater.*, 2020, 30.
3 H. Bysell, R. Mansson, P. Hansson and M. Malmsten, *Adv. Drug Delivery Rev.*, 2011, **63**, 1172–1185.
4 G. Agrawal, R. Agrawal and A. Pich, *Part. Part. Syst. Charact.*, 2017, **34**, 1700132.
5 W. Chen, Y. Hou, Z. Tu, L. Gao and R. Haag, *J. Controlled Release*, 2017, **259**, 160–167.
6 M. Karg, A. Pich, T. Hellweg, T. Hoare, L. A. Lyon, J. J. Crassous, D. Suzuki, R. A. Gumerov, S. Schneider, I. I. Potemkin and W. Richtering, *Langmuir*, 2019, **35**, 6231–6255.
7 N. Li, P. Zhao and D. Astruc, *Angew. Chem., Int. Ed.*, 2014, **53**, 1756–1789.
8 J. Liang, H. Wang and M. Libera, *Biomaterials*, 2019, **204**, 25–35.
9 S. Schmidt, M. Zeiser, T. Hellweg, C. Duschl, A. Fery and H. Möhwald, *Adv. Funct. Mater.*, 2010, **20**, 3235–3243.
10 T. J. Paul, S. Rübel, M. Hildebrandt, A. K. Strzelczyk, C. Spormann, T. K. Lindhorst and S. Schmidt, *ACS Appl. Mater. Interfaces*, 2019, **11**, 26674–26683.
11 F. Schröer, T. J. Paul, D. Wilms, T. H. Saatkamp, N. Jäck, J. Müller, A. K. Strzelczyk and S. Schmidt, *Molecules*, 2021, **26**(2), 263, DOI: 10.3390/molecules26020263.
12 D. Wilms, F. Schröer, T. J. Paul and S. Schmidt, *Langmuir*, 2020, **36**(42), 12555–12562.
13 K. Uhlig, T. Wegener, J. He, M. Zeiser, J. Bookhold, I. Dewald, N. Godino, M. Jaeger, T. Hellweg, A. Fery and C. Duschl, *Biomacromolecules*, 2016, **17**, 1110–1116.
14 A. Pich and W. Richtering, in *Chemical Design of Responsive Microgels*, ed. A. Pich and W. Richtering, Springer-Verlag Berlin, Berlin, 2010, vol. 234, pp. 1–37.
15 T. J. Paul, A. K. Strzelczyk and S. Schmidt, *Macromol. Biosci.*, 2021, **21**(4), 2000386, DOI: 10.1002/mabi.202000386.
16 D. Suzuki, K. Horigome, T. Kureha, S. Matsui and T. Watanabe, *Polym. J.*, 2017, **49**, 695–702.
17 M. Cors, O. Wrede, A.-C. Genix, D. Anselmetti, J. Oberdisse and T. Hellweg, *Langmuir*, 2017, **33**, 6804–6811.
18 S. Schmidt, T. Hellweg and R. von Klitzing, *Langmuir*, 2008, **24**, 12595–12602.
19 T. Cai, M. Marquez and Z. Hu, *Langmuir*, 2007, **23**, 8663–8666.
20 K. Kratz, T. Hellweg and W. Eimer, *Polymer*, 2001, **42**, 6631–6639.
21 K. Gawlitza, A. Radulescu, R. von Klitzing and S. Wellert, *Polymer*, 2014, **55**, 6717–6724.
22 A. Burmistrova, M. Richter, C. Uzum and R. von Klitzing, *Colloid Polym. Sci.*, 2011, **289**, 613–624.
23 S. Backes and R. Von Klitzing, *Polymers*, 2018, 10.
24 N. Welsch and L. A. Lyon, *PLoS One*, 2017, **12**, e0181369.
25 J. Dubbert, T. Honold, J. S. Pedersen, A. Radulescu, M. Drechsler, M. Karg and W. Richtering, *Macromolecules*, 2014, **47**, 8700–8708.
26 O. L. Virtanen, A. Mourran, P. T. Pinard and W. Richtering, *Soft Matter*, 2016, **12**, 3919–3928.
27 J. Gao and B. J. Frisken, *Langmuir*, 2003, **19**, 5217–5222.
28 M. F. Schulte, S. Bochenek, M. Brugnoni, A. Scotti, A. Mourran and W. Richtering, *Angew. Chem., Int. Ed.*, 2021, **60**, 2280–2287.
29 J. Gao and B. J. Frisken, *Langmuir*, 2003, **19**, 5212–5216.
30 H. Bachman, A. C. Brown, K. C. Clarke, K. S. Dhada, A. Douglas, C. E. Hansen, E. Herman, J. S. Hyatt, P. Kodlekere, Z. Y. Meng, S. Saxena, M. W. Spears, N. Welsch and L. A. Lyon, *Soft Matter*, 2015, **11**, 2018–2028.
31 M. A. Cooperstein and H. E. Canavan, *Biointerphases*, 2013, **8**, 19.
32 J.-F. Lutz, Ö. Akdemir and A. Hoth, *J. Am. Chem. Soc.*, 2006, **128**, 13046–13047.
33 K. Susumu, B. C. Mei and H. Mattoussi, *Nat. Protoc.*, 2009, **4**, 424–436.
34 O. L. J. Virtanen and W. Richtering, *Colloid Polym. Sci.*, 2014, **292**, 1743–1756.
35 D. Nečas and P. Klapetek, *Open Phys.*, 2012, **10**, 181–188.
36 E. K. Dimitriadis, F. Horkay, J. Maresca, B. Kachar and R. S. Chadwick, *Biophys. J.*, 2002, **82**, 2798–2810.
37 P. Carl, Radial Profile Plugin Extended, http://questpharma.u-strasbg.fr/html/radial-profile-ext.html, (accessed 12.12.2020, 2020).
38 M. Daoud, J. P. Cotton, B. Farnoux, G. Jannink, G. Sarma, H. Benoit, C. Duplessix, C. Picot and P. G. de Gennes, *Macromolecules*, 1975, **8**, 804–818.
39 P. G. De Gennes, *Macromolecules*, 1976, **9**, 587–593.
40 G. Li, I. Varga, A. Kardos, I. Dobryden and P. M. Claesson, *Langmuir*, 2021, **37**(5), 1902–1912.
41 M. Stieger, W. Richtering, J. S. Pedersen and P. Lindner, *J. Chem. Phys.*, 2004, **120**, 6197–6206.
42 S. Bergmann, O. Wrede, T. Huser and T. Hellweg, *Phys. Chem. Chem. Phys.*, 2018, **20**, 5074–5083.
43 D. Pussak, D. Ponader, S. Mosca, T. Pompe, L. Hartmann and S. Schmidt, *Langmuir*, 2014, **30**, 6142–6150.
44 A. Rubiano, C. Galitz and C. S. Simmons, *Tissue Eng., Part C*, 2019, **25**, 619–629.
45 M. F. Schulte, A. Scotti, M. Brugnoni, S. Bochenek, A. Mourran and W. Richtering, *Langmuir*, 2019, **35**, 14769–14781.
46 K. Kratz, A. Lapp, W. Eimer and T. Hellweg, *Colloids Surf., A*, 2002, **197**, 55–67.
47 J.-F. Lutz, *J. Polym. Sci., Part A: Polym. Chem.*, 2008, **46**, 3459–3470.